A comparison of methods to simulate the aerodynamic flow beneath a high speed train

Soper, David; Flynn, Dominic; Baker, Christopher; Jackson, Adam; Hemida, Hassan

DOI:
10.1177/0954409717734090

A comparison of methods to simulate the aerodynamic flow beneath a high speed train

David Soper, Dominic Flynn, Chris Baker, Adam Jackson, Hassan Hemida
University of Birmingham, UK

Abstract

The introduction of dedicated high speed railway lines around the world has led to issues associated with running trains at very high speeds. Aerodynamic effects increase proportionally with air speed squared, consequently at higher speeds aerodynamic effects will be significantly greater than for trains travelling at lower speeds. On ballasted trackbeds the phenomenon in which ballast particles become airborne during the passage of a high speed train has led to the need for understanding of the processes involved in train and track interaction (both aerodynamical and geotechnical). The difficulty of making full-scale aerodynamic measurements beneath a high speed train has created a requirement to be able to accurately simulate these complex aerodynamic flows at model-scale. In this study results from moving-model tests and numerical simulations were analysed to determine the performance of each method for simulating the aerodynamic flow underneath a high-speed train. Validation was provided for both cases by juxtaposing results against those from full-scale measurements. The moving-model tests and numerical simulations were performed at $1/25^{th}$ scale. Horizontal velocities from the moving-model tests and computational fluid dynamics (CFD) simulations were mostly comparable except those obtained close to the ballast. In this region the multi-hole aerodynamic probes were unable to accurately measure velocities. The numerical simulations were able to resolve the flow to much smaller turbulent scales than could be measured in the experiments, and showed an overshoot in peak velocity magnitudes. Pressure and velocity magnitudes were found to be greater in the numerical simulations than the experimental tests. This is thought to be due to the influence of ballast stones in the experimental studies allowing flow to diffuse through them; whereas, in the CFD simulations the flow stagnated on a smooth non-porous surface. Additional validation of standard deviations and turbulence intensities found good agreement between the experimental data but an overshoot in the numerical simulations. Both moving model and CFD techniques were shown to be able to replicate the flow development beneath a high-speed train. These techniques could therefore be used as a method to model underbody flow with a view to train homologation.

Nomenclature

δ	CFD time step length	U_{res}	overall normalised horizontal velocity
$\Delta\ x$, $\Delta\ y$, $\Delta\ z$	smallest cell sizes in the x, y and z directions	V	ensemble mean of lateral slipstream velocity, normalised by train speed
Re	Reynolds number	v	ensemble mean of lateral slipstream velocity (m/s)
ν	kinematic viscosity	V_{train}	train speed (m/s)
Ψ	Sweby limiter	W	ensemble mean of vertical slipstream velocity, normalised by train speed
ρ	air density (kg/m^3)	w	ensemble mean of vertical slipstream velocity (m/s)
τ	normalised time scale	x	distance measured from vehicle nose along the track (m)
$\tilde{\Delta}$	CFD filter width	y	distance measured normal to the track from the centre of track (m)
C_P	coefficient of pressure	y^*	distance from the wall to the adjacent node
L_{train}	train length (m)	z	distance measured from the top of the rail in the vertical direction (m)
N	number of independent runs conducted	H	model scale train height (m)
p	pressure (Pa)	y$^+$	non-dimensional wall-normal distance
p_0	ambient pressure (Pa)		
U	ensemble mean of longitudinal slipstream velocity, normalised by train speed		
u	ensemble mean of longitudinal slipstream velocity (m/s)		
u^*	friction velocity		

1 Introduction

High speed railways have become a familiar sight around the world and allow trains to operate at speeds over 300 kph. In countries such as South Korea and China train speeds have steadily increased over time and the infrastructure is now capable of coping with train speeds approaching 400 kph. There are many issues associated with running trains at very high speeds which include infrastructure development, train design and maintenance. Aerodynamic effects increase proportionally with air speed squared, consequently at higher speeds aerodynamic effects will be significantly greater than for trains travelling at lower speeds.

There are two methods of constructing the ground surface on which the sleepers and rails on a high speed railway are mounted: slabtrack or a ballasted bed. Slabtrack is made from concrete slabs and is generally considered

a more permanent structure, requiring less maintenance than a ballasted bed although it is inherently more expensive to implement. Ballasted track is easier and cheaper to install than slabtrack but requires regular maintenance and can lead to issues such as 'ballast projection'.

Ballast projection is the phenomenon by which ballast particles become airborne during the passage of a high speed train and was first observed on Japanese and Korean high speed railways [1]. Flying ballast particles can cause extensive damage to the underbody of trains and to the rail head if crushed between a wheel and the rail. Figure 1, replicated from Quinn et al. [2], shows ballast pitting damage as a result of a ballast particle being crushed on the rail head. Further evidence of ballast flight is often cited as damaged wheel sets, broken glass in stations and damaged acoustic trackside screens. On high speed rail networks the effects of ballast crushing on the rail head is significant as the forces involved are large enough to cause permanent deformation of the rail. This in turn may create 'voiding' or hollow areas in the ballast between sleepers downstream of an uncorrected deformation [2].

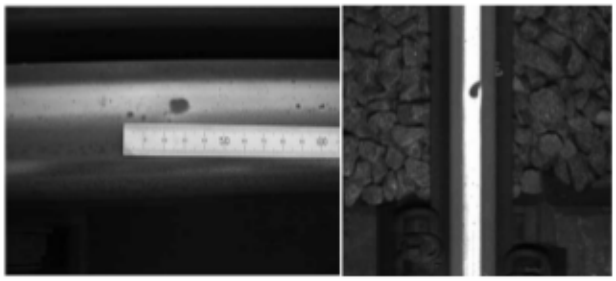

Figure 1: Ballast pitting damage as observed during a manual track inspection (left) and from an automatic detection system (right). Image replicated from Quinn et al. [2].

It is thought that ballast projection is caused by a combination of high air speeds beneath a train and mechanical excitation of the ground during

a train passage. The train underbody is usually the 'roughest' surface of the vehicle due to the irregular shapes and discontinuities caused by the mounting of the bogies, underbody equipment and inter-carriage gaps. The underbody flow is also influenced by the presence of the ground as a containing surface, and as such the flow is generally characterised as a highly turbulent Couette type flow that is sensitive to vehicle geometry [2]. European codes of practice outline limits for pressure loading amplitudes on trackside structures, however they do not extend to a standardised methodology and prescribed limit values for measured loads on the track bed [3]. As such ballast projection is still an open point within the European Technical Specifications for Interoperability (TSI) [3].

Previous studies of the aerodynamic flow underneath a train have been limited and so far the focus has been mainly on characterising the processes involved in the initiation of ballast projection. Furthermore, few studies cite the potential link between aerodynamic and geotechnical processes as the cause of ballast projection. Research has mainly been undertaken in countries were trains speeds are reaching 300 kph, such as Japan, Korea, Germany, France, Spain, Italy and the UK [4, 1, 5, 2]. These studies have characterised the aerodynamic flow underneath a high speed train by measuring the velocity and pressure field entrained between the tracks. Methodologies adopted by each study are quite different and include full-scale tests [1, 6, 5, 2], model-scale simulations [4, 7]and CFD simulations [6, 8]. Slipstream velocities have shown an annular type flow underneath a train where velocities increase in magnitude with height above the sleeper surface [1]. In these cases, peak velocities are observed at the centre of track which fall away with lateral position [1].

Data from many of the studies was used to develop mathematical models

of the ballast flight phenomenon [2, 5, 9, 10, 11], while also providing validation for model-scale experiments and CFD simulations [6, 8]. In general, simulations of the aerodynamic flow underneath a train have been highly simplified due to the complexities of the train and track geometries. To simulate train movement in relation to the ground, moving ground belts in wind tunnels and moving models have been used although results have failed to accurately simulate the underbody flow conditions [4, 12]. Recently, increases in computational power have made the study of vehicle aerodynamics by CFD more accessible. However, the complexities of simulating flow around a high speed train has often meant simulations are highly simplified and only undertaken for small sections of a train. Differences between results when validated against full-scale data has led to uncertainty in the application of CFD for studying ballast projection [6].

The work presented in this paper is part of a large EPSRC funded project between the Universities of Southampton and Birmingham entitled 'Track systems for high speed railways: Getting it right', to look at various aspects of high speed track. Aerodynamic studies were undertaken to characterise the flow development underneath a high speed train by conducting full-scale experiments, as well as scaled model experiments and CFD simulations. The full-scale measurements were conducted concurrently with geotechnical measurements made by the University of Southampton to allow all of the forces applied to a ballast particle during the passage of a train to be quantified. These results will be reported in an accompanying paper, assessing the influence of each major force on a ballast particle and developing an analytical method to deduce the type of motion the particle could be initiated into [13]. This paper focuses on the model-scale experiments and CFD simulations. Full-scale experiments are usually expensive and difficult to complete, with

results highly susceptible to changes in ambient conditions. Model-scale experiments and CFD simulations offer a cheaper and easier alternative method for understanding slipstream development in greater detail. Due to issues such as scaling effects and differing methodologies results need validation. The experimental and CFD setups used in this study are described in detail, along with the data analysis techniques. Results for pressure and velocities are presented separately for each simulation technique and thoroughly validated against full-scale data. Finally, each simulation technique is discussed in relation to suitability of modelling the underbody flow and assessed in light of the current need for train homologation.

2 Physical modelling methodology

2.1 TRAIN rig

Modelling the relative movement between a train with respect to the ground has been problematic in previous train underbody studies [4, 12] due to the type of moving/non-moving methods employed and the confined nature of the space in which the measurements are made leading to unrealistic results being produced. The University of Birmingham TRansient Aerodynamic INvestigation (TRAIN) rig is a moving-model facility, purpose-built to examine the transient aerodynamics of moving vehicles [14]. Scaled model vehicles are propelled at speeds up to 75 m/s, dependent on model weight, along a 150 m track. The moving-model facility negates the issue observed in previous studies as it accurately simulates the movement of a vehicle with respect to a fixed ground plane.

The facility was designed and built by British Rail in the early 1990s primarily for examining the effects of trains passing through tunnels. The

Figure 2: The concrete base of the testing rig.

model runs along a track that is mounted to a 0.15 m thick permanent concrete base which spans the entire length of the test rig, as shown in figure 2. This concrete base, along with the firing mechanism [15], prevents measurements from being made underneath the train. To overcome this limitation, a novel approach was applied in this study by which the moving train was turned upside-down and run past a ground plane modelled as a suspended floor above the normal running tracks. Figure 3 shows the suspended ground plane with the upside-down model train passing beneath.

The suspended floor was an accurately modelled representation of the full-scale experiment site on a high speed railway in the UK[13]. The ground plane is modelled with a single track running down the centre, with a 0.028 m ballast shoulder (0.7 m at full-scale) on one side and flat ground on the other. The ground plane extends 10 m in length and is set at a height 0.17 m above the normal running track. The setup represents one half of a typical twin track section of high speed railway modelled at $1/25^{th}$ scale. The bed of ballast particles at full-scale creates a rough boundary for the flow underneath a train. After analysing typical ballast particle sizes it was found that fish tank gravel was a suitable size to simulate individual ballast

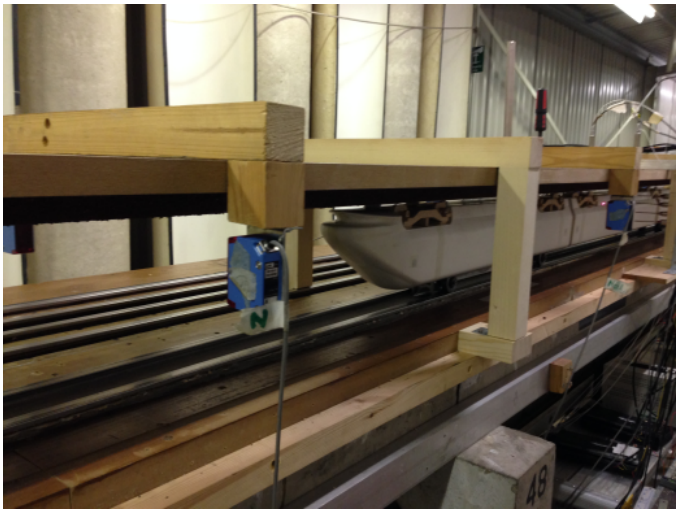

Figure 3: The upside-down ground plain with Class 373 Eurostar model and measuring instrumentation.

particles at $1/25^{th}$ scale.

The ground plane enabled measurement instrumentation to be easily set up in the space between the ballast level and the underside of the model train. A 2.5 mm gap, through which instruments could be set up was cut across the ground plane at a position 7 m from the start of the plane. This position was chosen to allow the boundary layer between the train and the ground plane to fully develop, while also preventing the downstream end of the ground plane from adversely affecting the results.

Further information regarding the general set up of the TRAIN rig and modelling techniques used can be found in Soper et al. [15].

2.2 TRAIN rig model

The experiment was conducted using a $1/25^{th}$ scale model Class 373 Eurostar high speed train, specifically designed to run upside-down (figure 5). The Class 373 Eurostar was chosen for this experiment to enable com-

Figure 4: The multi-hole probe setup through the ground plane. The slit through which the instrumentation was placed is clearly visible, as is the simulated ballast roughness.

parisons to be made with full-scale data collected on HS1, UK [16]. The Eurostar model was designed to run in either a six or seven car configuration to investigate findings from the full-scale data relating to different vehicle bogie positions. The Glass Reinforced Plastic (GRP) model was accurately constructed to be an exact representation of the computer-aided design (CAD) model used in the CFD simulations; the CAD model was in turn an accurate but simplified representation of an actual Class 373. Highly detailed components, such as bogies, were geometrically simplified to be modelled in balsa wood. The Class 373 Eurostar has a number of different inter-carriage spacing and bogie types which are shown in figure 6. Previous studies have indicated that the inter-carriage regions create peaks in aerodynamic properties of the flow; thus care has been taken to accurately model such components [2].

The upside-down model was mounted to a specially designed chassis and trailing wheel system which evenly spread the weight of the model and

Figure 5: The TRAIN rig Class 373 Eurostar 7 car model.

(a) Standard bogie inter-carriage region

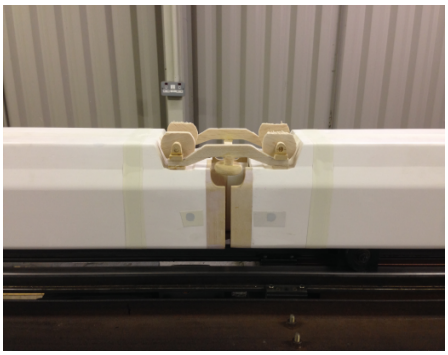

(b) Articulated bogie inter-carriage region

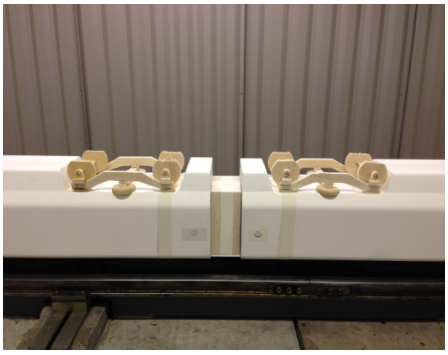

(c) Centre bogie inter-carriage region

Figure 6: The different types of bogie on a Class 373 Eurostar.

gave stability and a means of attaching the propulsion/braking devices [15]. Mounting the model on a rigid chassis also prevents excessive lateral and vertical motion, which was important for this study because the model ran within 2 mm of the suspended ground plane.

A nominal train speed of V_{train} = 41.67 m/s was chosen for these tests. The nominal train speed is half the maximum full-scale train speed V_{train} = 83.67 m/s (300 kph) however, comparisons with full-scale data, shown later, demonstrate good agreement for normalised magnitudes, indicating Reynolds number independence within the ranges examined. The Reynolds number for a $1/25^{th}$ scale train travelling at 41.67 m/s with a characteristic height of 0.156 m is 4.4x10^5. However, as this is essentially a turbulent, rough-walled cavity flow, a more appropriate Reynolds number is based on the distance between the rails is 1.62x10^5.

2.3 Instrumentation and analysis methodology

The model-scale and CFD simulations will be validated against data from a series of full-scale experiments conducted on HS1, UK [16]. The full-scale tests used rakes of pitot-static tubes to measure the total horizontal velocity for a range of heights and lateral positions, as well as static pressure probes close to the ballast bed for different lateral positions. The positions of the multi-hole probes and static pressure taps used in the model-scale tests were chosen to replicate the types of data recorded at full-scale.

2.3.1 Multi-hole probes

Multi-hole pressure probes, manufactured by Turbulent Flow Instrumentation [17], were used to measure the aerodynamic flows in the model-scale experiment. The probes are capable of measuring local static pressure and

three components of velocity instantaneously, within calibrated bounds of ±0.5 m/s, ±5 Pa and ±1° for velocities, static pressure and flow direction respectively. The probes are designed to measure turbulent air flows in a wind tunnel within a ±45° cone of acceptance. The restriction on the angle of flow detection is a drawback within the highly 3-dimensional aerodynamic flow beneath a high speed train. Measurements were made at a sampling frequency of 5000 Hz. All data was filtered using a 650 Hz low-pass filter to reflect the maximum frequency response of the probe and all data below 2 m/s were discarded due to a minimal flow cut-off condition [15]. All data was resampled with respect to a nominal train speed (V_{train} = 41.67 m/s) to account for small differences in speed between test runs.

Multi-hole probe measurements were made at a series of lateral and vertical positions from centre of track (COT) and above top of rail (TOR), as indicated in table 1. The measuring positions were chosen to replicate those from the full-scale experiments as closely as possible and offer a detailed array of positions beneath the train to aid understanding of the flow development.

2.3.2 Static pressure taps

Static pressures were measured on the ballasted track bed using First Sensor HCLA type pressure transducers connected to a short length of rubber tubing fed into the ground plane instrumentation gap until flush with the ballast level. A common reference pressure, sourced from an area outside of the influence of the passing model, was used for all transducers. The ranges of the pressure transducers were optimised based on the peak pressures measured during a series of preliminary experiments. Data was recorded using a Measurement Computing LGR-5325 type stand-alone data logger at a sam-

	Distance from centre of track (m)								
Distance from top of rail (m)	-2.312	-1.085	-0.41	0	0.41	1.085	2.312	3.0	3.625
0.11	-	-	X	X	X	-	-	-	-
0.05	-	-	X	X	X	-	-	-	-
-0.018	-	-	X	X	X	-	-	-	-
-0.09	-	-	X	X	X	-	-	-	-
-0.14	-	-	X	X	X	-	-	-	-
0.092	X	X	-	-	-	X	X	-	-
0.024	-	X	-	-	-	X	X	-	-
-0.048	-	X	-	-	-	X	X	-	-
-0.098	-	X	-	-	-	X	X	-	-
-0.136	X	X	-	-	-	X	X	-	-
0	-	-	-	-	-	-	-	X	-
0.2	-	-	-	-	-	-	-	X	X
0.8	-	-	-	-	-	-	-	X	-
1.4	-	-	-	-	-	-	-	X	-
2.0	-	-	-	-	-	-	-	X	-

Table 1: Multi-hole probe measuring positions. All dimensions are given as the full-scale equivalent in metres. X indicates that a measurement was made at the selected position.

pling frequency of 2000 Hz. All pressure transducers were calibrated using a Betz 2500 micromanometer. A resonant frequency test was also performed to confirm that the tubing did not excessively distort the measured pressures. All data was resampled with respect to a nominal train speed (V_{train} = 41.67 m/s) to account for small differences in speed between runs. Static pressures were measured at 0.2 m (full-scale) intervals from centre of track in both directions. Atmospheric reference values used to non-dimensionalise pressure data were measured using a GBP3300 Digital Barometer and an Oregon Scientific BAR208HGA.

2.3.3 Light gates

Pairs of photoelectric position finders were used to measure train speed to an accuracy of ±0.1 m/s. Train speed was measured before and after the measurement instrumentation. The decrease in train speed over the mea-

surement site was 0.2 m/s which can be considered negligible. Additionally, a laser light gate was set up directly in line with the ground plane instrumentation to act as a position finder in the data and provide another point of reference for calculating train speed accurately at the instrumentation position. Light gate data was recorded on all data acquisition systems and therefore allowed pressure transducer and multi-hole probe data to be synchronised. Train speeds were measured to within ±3% of the nominal train speed. This meets the criteria set out by CEN [18], which in turn lie within the prescribed train speed measurement accuracy limits defined in TSI [3].

3 Computational fluid dynamics (CFD) methodology

3.1 Domain and boundary conditions

The computational domain used in this work is shown in figure 7. The domain blockage ratio is 0.5% which is significantly lower than the 5% value suggested by CEN [18]. This ensures that there is sufficient distance between the train and the boundary conditions to prevent any unwanted interactions between them and the flow around the train. The outlet of the domain is positioned 58H behind the train, where H is the train height (H=0.156 m at 1/25th scale). The positioning of the outlet is important as pressure fluctuations created in the vehicle wake can cause numerical instabilities for the zero-pressure outlet condition. The distance between the train and the outlet boundary provides sufficient distance for the wake pressure to dissipate before it reaches the outlet.

The ground plane was defined as a moving wall with the same velocity as the inlet to replicate the correct relative movement between the train

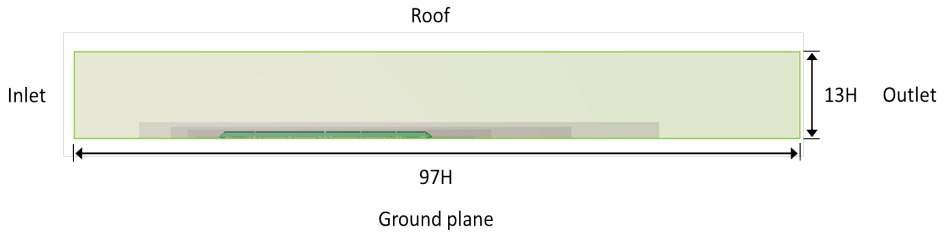

Figure 7: Computational domain used in the simulations.

and the ground. This method has been widely used in CFD studies of train aerodynamics [19, 20] because it is less complex than the alternative method of using sliding meshes. It should be noted that, like the train, the ground plane is a smooth no-slip wall. This contrasts with the moving model tests which used scaled ballast particles to give the ground plane a relative roughness comparable to the full-scale case. The sides and roof of the domain are defined as slip walls to prevent boundary layer growth which would adversely affect the flow within the domain.

The inlet is defined as a uniform velocity profile at a nominal speed of $V_{train} = 40$ m/s, similar to that used in the model-scale tests. As the CFD and model-scale geometries were both 1/25th scale, the Reynolds numbers in the two cases were closely matched.

The origin in the CFD simulations is taken as being at the front face of the train, COT and the TOR in the x, y and z directions, respectively. This coordinate system is also adopted in the experimental studies.

3.2 Simulation method

The CFD results presented in this work were obtained using large-eddy simulation (LES) which can provide enormous quantities of high resolution data from a single simulation with a minimum of user effort. However,

LES has a massive associated computational cost in comparison to the more commonly-used Reynolds-averaged Navier-Stokes (RANS) methods which only provide mean flow data. The principle of LES is that the larger turbulent scales within a flow are directly resolved and the influence of the smaller, dissipative scales, is modelled. The scales that are modelled are smaller than the 'filter width' which is defined as

$$\tilde{\Delta} = (\Delta x \Delta y \Delta z)^{\frac{1}{3}} \tag{1}$$

where Δx, Δy and Δz are the smallest cell sizes in the x, y and z directions. The standard isochoric Smagorinsky model was used in the simulations to represent the behaviour of the sub-grid scales. This has been used successfully in previous train aerodynamics simulations [19, 20, 21]. Van Driest damping was applied to the train surface and ground plane to ensure that unphysical turbulence was not produced.

3.3 Numerical Schemes

The LES were conducted using the open-source finite volume CFD code OpenFOAM version 2.3.0. The diffusive and sub-grid fluxes were discretised using a second order central-differencing scheme. The convective term was discretised using central-differencing with a Sweby limiter [22] to form a total variation diminishing (TVD) scheme; the limiter was set to Ψ=1 which gave full TVD conformance. In commercial codes, this convection scheme is commonly known as 'bounded central differencing'. Time integration was conducted using a second order backward implicit scheme. The mean Courant-Friedrichs-Lewy (CFL) number in the simulations was 0.007 and the maximum CFL number was kept below 1 in all cells at the cost of

requiring a time step of Δ t = 5x10^{-6} s.

Time-averaging of pressure and velocity was commenced once the flow was fully-developed which was determined by examining the massive array of sampling probes placed beneath the train and ensuring that the values fluctuated about a mean quantity. Time-averaging was conducted for the time required for the flow to travel the length the entire train eight times, giving an equivalent full-scale time of 14 s which ensured that the motion of the lower-frequency turbulent fluctuations were incorporated in the average.

3.4 Computational mesh

The mesh used for the numerical simulations was an unstructured finite volume grid generated using $HEXPRESS^{\text{TM}}$/Hybrid. The coarse and fine meshes consisted of 16 and 27 million cells, respectively. Figure 8 shows the fine mesh projected onto a plane at the centre of track. The mesh size is relatively coarse in comparison to other train aerodynamics work using LES or DES [19, 20, 23], although the mesh has been refined underneath the train, where the flow behaviour is considered most important in this study.

The resolution of the boundary layer on a surface is essential to ensure that the flow is correctly modelled. In LES the boundary layer must be resolved down to the laminar sublayer to ensure accurate modelling of the near wall flow phenomena in the boundary layer. The non-dimensional wall-normal distance y^+ is used to determine the distance of the first node adjacent to the train surface and ground plane where

$$y^+ = \frac{u^* y^*}{\nu} \tag{2}$$

where u^* is the friction velocity, y^* is the distance from the wall to the adja-

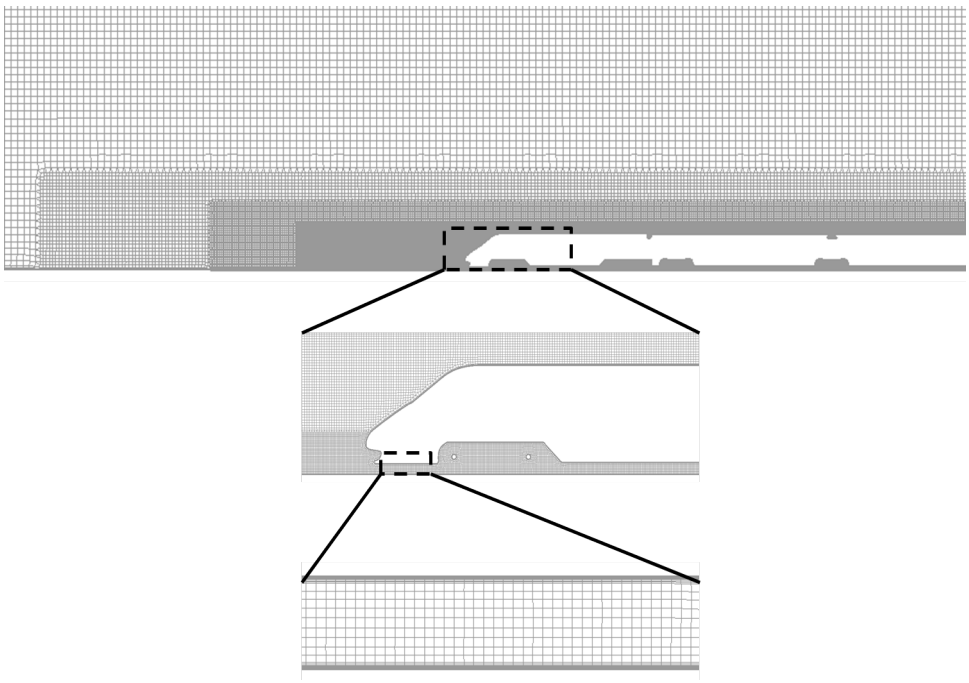

Figure 8: Computational mesh projected onto a cut plane at COT.

cent node and ν is the kinematic viscosity. In the simulations the first node adjacent to the ground plane and train is typically at $y^+ \leq 2$. The unsteady flow can cause transient increases in y^+; at all times the y^+ remained below 11.

In order to consider an LES to be 'good', Pope[24] suggested that 80% of the turbulence kinetic energy (TKE) should be directly resolved. Figure 9 shows the percentage of resolved TKE in the flow beneath the train at three positions. It can be seen that for the majority of train length, more that 90% of the TKE is resolved. Ahead of the train this value drops significantly due to flow separating around the edge of the rails causing an increase in sub-grid viscosity. Nevertheless, for almost the entire train length a substantial portion of the TKE is directly resolved.

Figure 10 shows a comparison between pressure coefficients and nor-

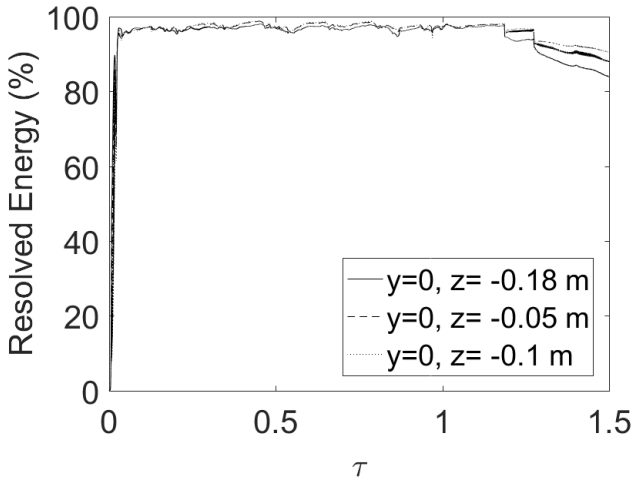

Figure 9: Percentage of turbulence kinetic energy that is directly resolved at COT for z=-0.18 m, -0.1 m and -0.05 m.

malised longitudinal velocity components from the coarse and fine meshes at the COT for measuring position $z = 0.05$ m. The data agree very closely for the majority of train length however there is slight discrepancy at the second intercarriage gaps. The fine mesh has approximately double the number of cells as the coarse mesh and therefore the flow will not change with further mesh resolution, considering the level of resolved TKE.

4 Data analysis methodology

As results from both underbody flow simulations will be validated against full-scale data it is important to ensure that the methods of data analysis are consistent and that fair comparisons can be made. The highly turbulent nature of the transient aerodynamic flow beneath a high speed train enforces the use of ensemble averaging techniques. The European TSI states that to validate results for aerodynamic flows an experiment should be repeated at least 20 times for velocity measurements and at least 10 times for static

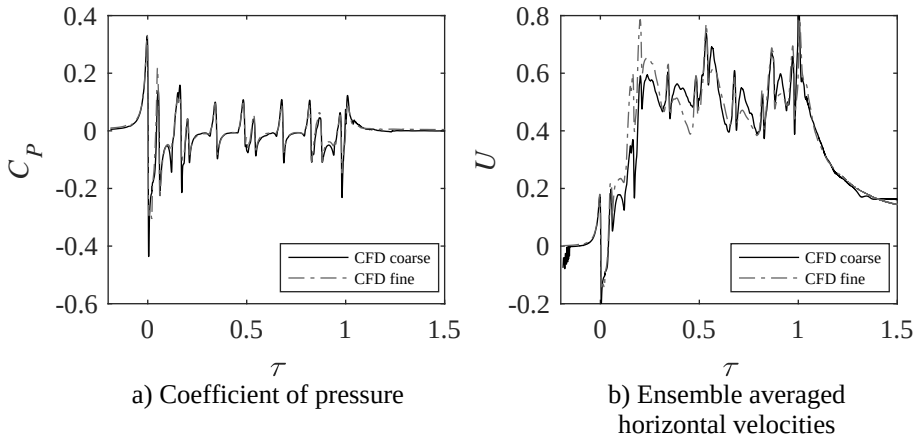

a) Coefficient of pressure

b) Ensemble averaged horizontal velocities

Figure 10: Comparison of mesh sensitivity for the coefficient of pressure and normalised velocity components at COT for measuring position z=0.05 m.

pressure measurements [3]. Ensemble averaging techniques can be applied easily to the model-scale data; however, the nature of CFD simulations makes this sort of analysis difficult.

Time-averaging in CFD is conducted arithmetically at each time-step until a point where the 'mean flow' does not change. An alternative method proposed by Flynn et al.,[20] took instantaneous velocities along sampling lines in the domain at random and sufficiently-spaced times, producing velocity signals that were analogous to those obtained from full-scale or moving model tests. From these instantaneous velocity samples, ensemble averages can be formed.

Properties of the aerodynamic flow are presented as non-dimensional

coefficients to aid comparison of results,

$$U(\tau) = \frac{u(\tau)}{V_{train}} \tag{3}$$

$$V(\tau) = \frac{v(\tau)}{V_{train}} \tag{4}$$

$$W(\tau) = \frac{w(\tau)}{V_{train}} \tag{5}$$

$$U_{res}(\tau) = \sqrt{\left(\frac{u(\tau)}{V_{train}}\right)^2 + \left(\frac{v(\tau)}{V_{train}}\right)^2} \tag{6}$$

$$C_P(\tau) = \frac{p(\tau) - p_0}{\frac{1}{2}\rho V_{train}} \tag{7}$$

where τ is a normalised time scale such that $\tau = 0$ occurs at the train nose and $\tau = 1$ occurs at the train end. U_{res} is the overall normalised horizontal velocity as measured in the full-scale experiments. The coefficient of pressure C_P is calculated at model-scale with respect to an ambient reference pressure, p_0, and the air density, ρ. The CFD simulations used in this work are incompressible and as such do not require a reference pressure. For the calculation of C_P from the numerical results, the reference pressure, p_0, will equal zero.

5 Results

5.1 Pressure measurements

Slipstream static pressures from beneath the train are directly compared against static pressures measured on the trackbed surface. Figure 11 shows model-scale results for the rake of measuring positions in the COT and those nearest to the rail outside of the 'four foot' (the region between the two running rails). The corresponding static pressures measured on the trackbed at comparable lateral positions are also plotted. Values measured for all

heights beneath the train are similar. The development of pressure follows a similar pattern to results observed at the train side [25], with characteristic changes in pressure around the train nose, tail and intercarriage gaps. Results from within the four foot have larger magnitudes than measurements made outside the running rails. It is possible to pick out influences from the vehicle geometry, such as individual bogie placements.

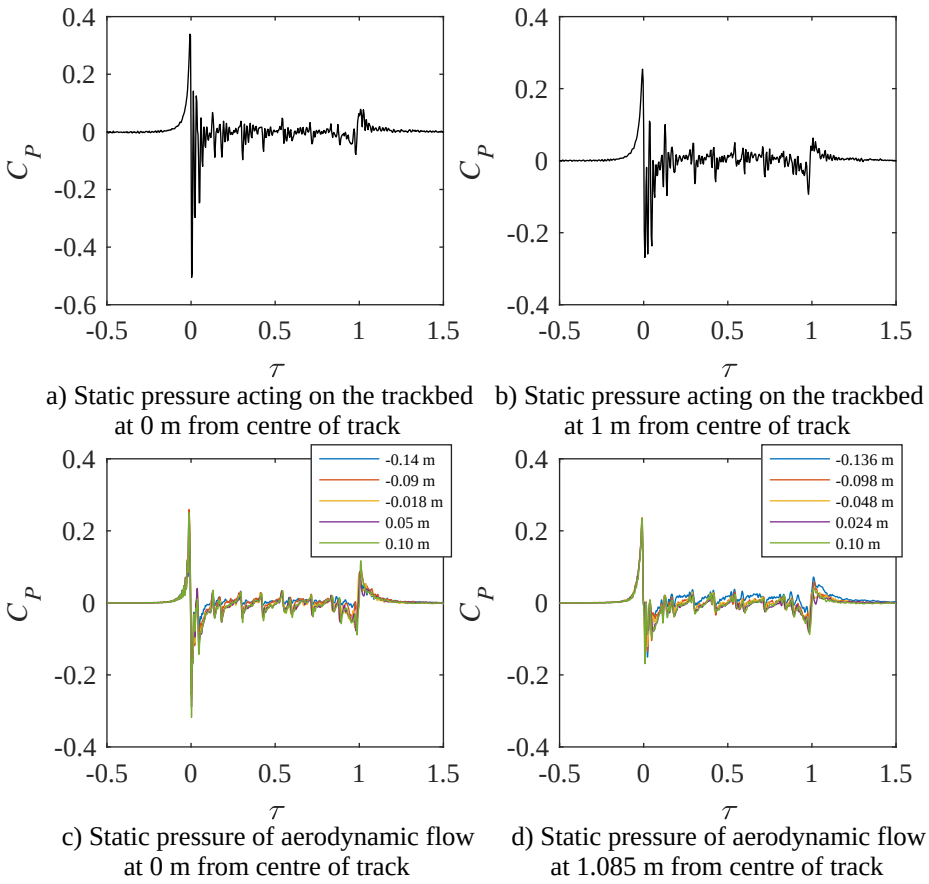

Figure 11: Coefficient of pressure C_P results on the trackbed for positions at 0 m and 1 m from centre of track. The corresponding C_P results for the rake of measuring positions at 0 m and 1.085 m from centre of track are also shown.

A comparison of static pressure results measured on the trackbed are shown for full-scale, model-scale and CFD data in figure 12. The full-scale

and CFD positions are measured at 0.158 m and 0.641 m from COT, whereas the model-scale data is measured at 0.2 m and 0.4 m. Analysis of model-scale results between 0 m and 1.0 m from COT indicated little difference in pressure development and peak magnitudes, thus the relatively small difference in measurement positions was considered acceptable for this comparison. Train lengths in the scaled simulations were much shorter than the full-scale train. As such data has been split in various locations and aligned with respect to matching bogie and intercarriage placements, hence the discontinuous lines in figure 12. Both simulations indicate similar flow

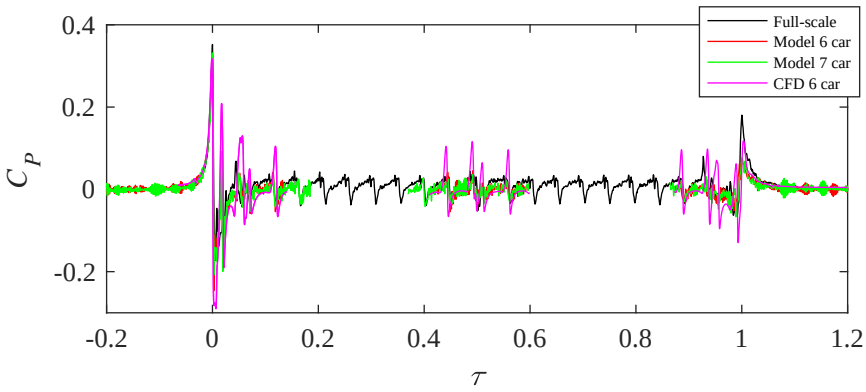

a) Trackbed static pressure at 0.16 m from centre of track

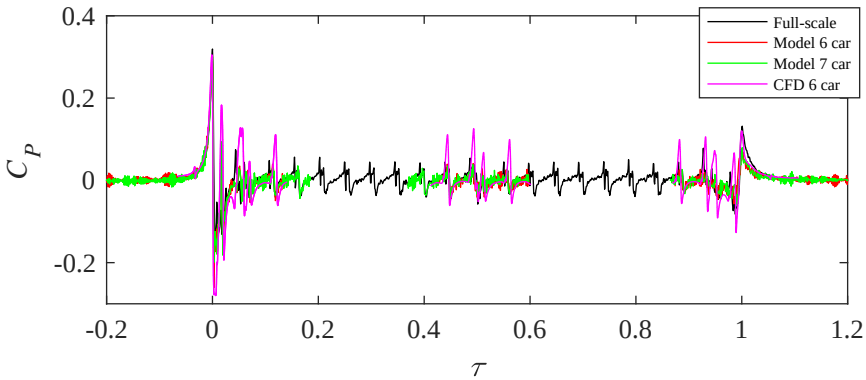

b) Trackbed static pressure at 0.64 m from centre of track

Figure 12: A comparison of coefficient of pressure C_P results for CFD, full-scale and model-scale data measured on the trackbed for positions 0.158 m and 0.641 m from centre of track.

development to full-scale results; however, CFD peak magnitudes overshoot values observed experimentally. In both full- and model scale experiments some form of ballast was present. This may be thought of as a semi-porous material, which will allow flow to move through it and not fully stagnate. Greater pressure magnitudes in the CFD simulations are thought to be due to flow stagnation on the smooth non-porous track surface, causing energy from the flow to be fully converted to pressure. Model-scale results suggest good agreement with full-scale data at the train nose and inter-carriage regions; however in the model-scale case the positive peak at the train tail is smaller in magnitude.

The influence of different bogie types and placement also has a clear effect on the pressure traces. The articulated bogie between two carriages creates a characteristic change in pressure with a positive then negative peak, similar to the nose region but much smaller in magnitude, figure 13b. The standard and central inter-carriage gaps have a bogie either side of the gap (figure 6). This creates two characteristic changes in pressures as shown in figure 13a and 13c. In both cases the magnitude of the pressure fluctuations are similar, but the central inter-carriage gap fluctuations are spread over a longer time period due to the larger spacing between carriages.

Figure 14 shows cut planes through the CFD predictions of pressure coefficient at TOR for the three bogie types. The pressure coefficients around the sides of the intercarriage gap are greater for the standard intercarriage gap. This is a result of the larger difference between the local air speed and the train speed. At the rear of the train, once the boundary layer has developed, values of pressure coefficient are much lower. In all cases a negative pressure region exists where the bogie region joins the underside of the carriage, with flow separation around the corner. In the case of the

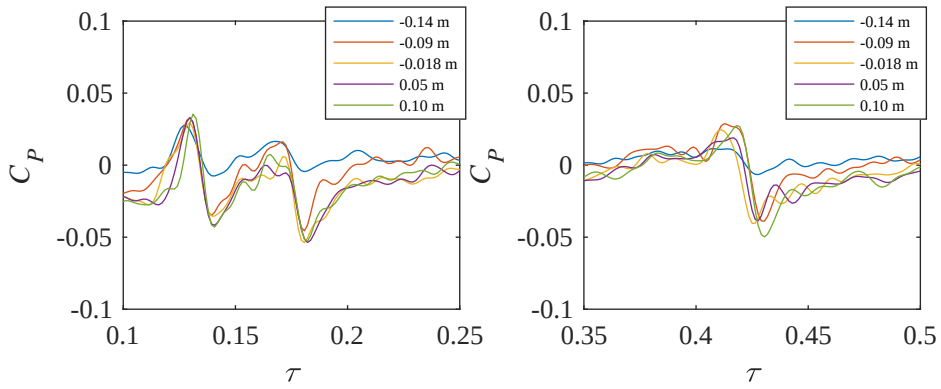

a) Standard intercarriage gap

b) Articulated intercarriage gap

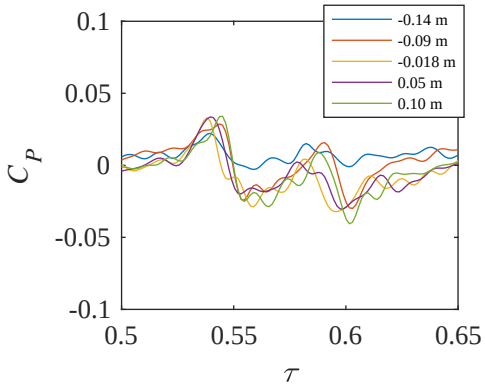

c) Central intercarriage gap

Figure 13: Model-scale individual bogie results for coefficient of pressure C_P measured at 0 m from centre of track.

articulated and standard intercarriage gaps a small positive pressure region occurs as a result of stagnation on the inclined face leading to the underside of the carriage.

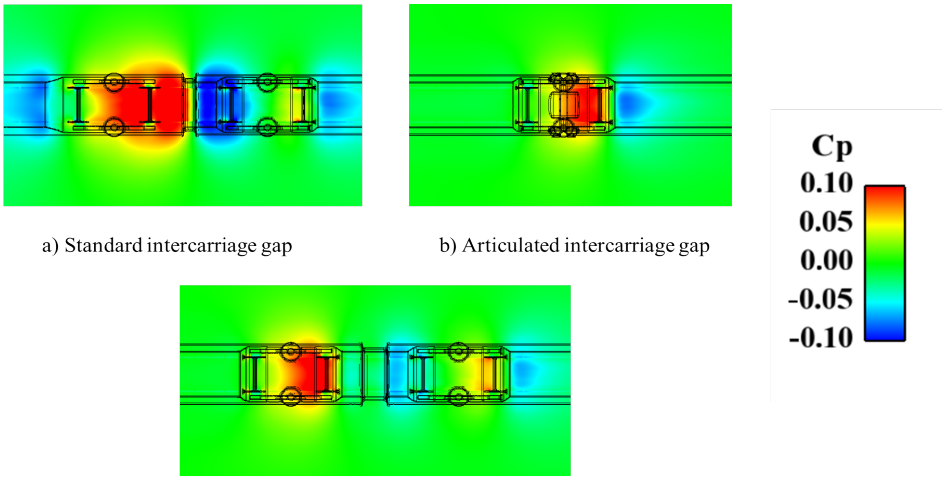

a) Standard intercarriage gap

b) Articulated intercarriage gap

c) Central intercarriage gap

Figure 14: Cut planes at 0 m from top of rail coloured by coefficient of pressure, C_P, for the three bogie types. Flow is moving left to right. Black lines are a projection of the geometry onto the cut plane, rather than an intersect through the geometry.

5.2 Velocity measurements

Figure 15 shows model-scale ensemble averaged total horizontal velocity traces for a series of heights above TOR (table 1) for the measuring position at COT and a position measured outside the four foot. Results presented are representative of all measurement positions analysed. It is clear that as the measuring height is increased the magnitude of slipstream velocities also increases; the flow can be considered to undergo typical boundary layer growth between the train and the ballasted trackbed. Unfortunately, the experimental studies were unable to get close enough to the train to measure any boundary layer effects on the underbody surface; however, this

effect has been captured in the CFD simulations. Figure 16 shows the time-average velocity on cut planes normal to the x axis at a number of different x positions. Boundary layer development is observed close to the trackbed with continued increasing velocities to V_{train} at the underbody surface of the train.

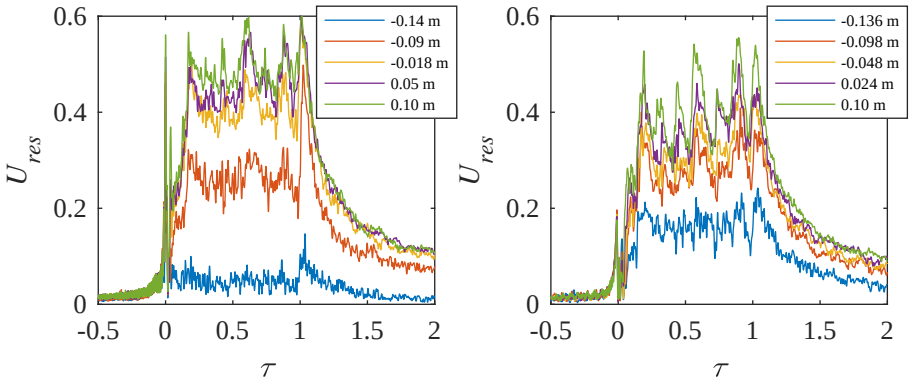

a) Ensemble horizontal velocities at 0 m from centre of track

b) Ensemble horizontal velocities at 1.085 m from centre of track

Figure 15: Ensemble averaged horizontal velocities U_{res} results for the rake of measuring positions at 0 m and 1.085 m from centre of track shown for the model-scale experiments.

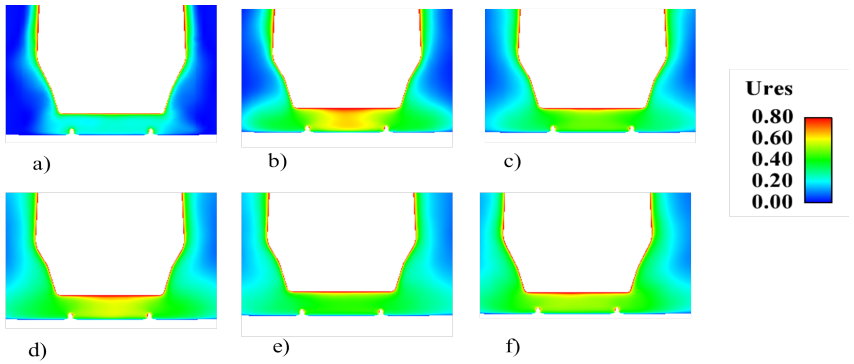

Figure 16: Time-averaged horizontal velocities U_{res} from the CFD simulations shown on cut planes normal to the x axis at the centre of cars 1-6 for a-f, respectively.

A comparison of results for the ensemble averaged total horizontal velocity measured at different heights above TOR at 0 m and 1.085 m from

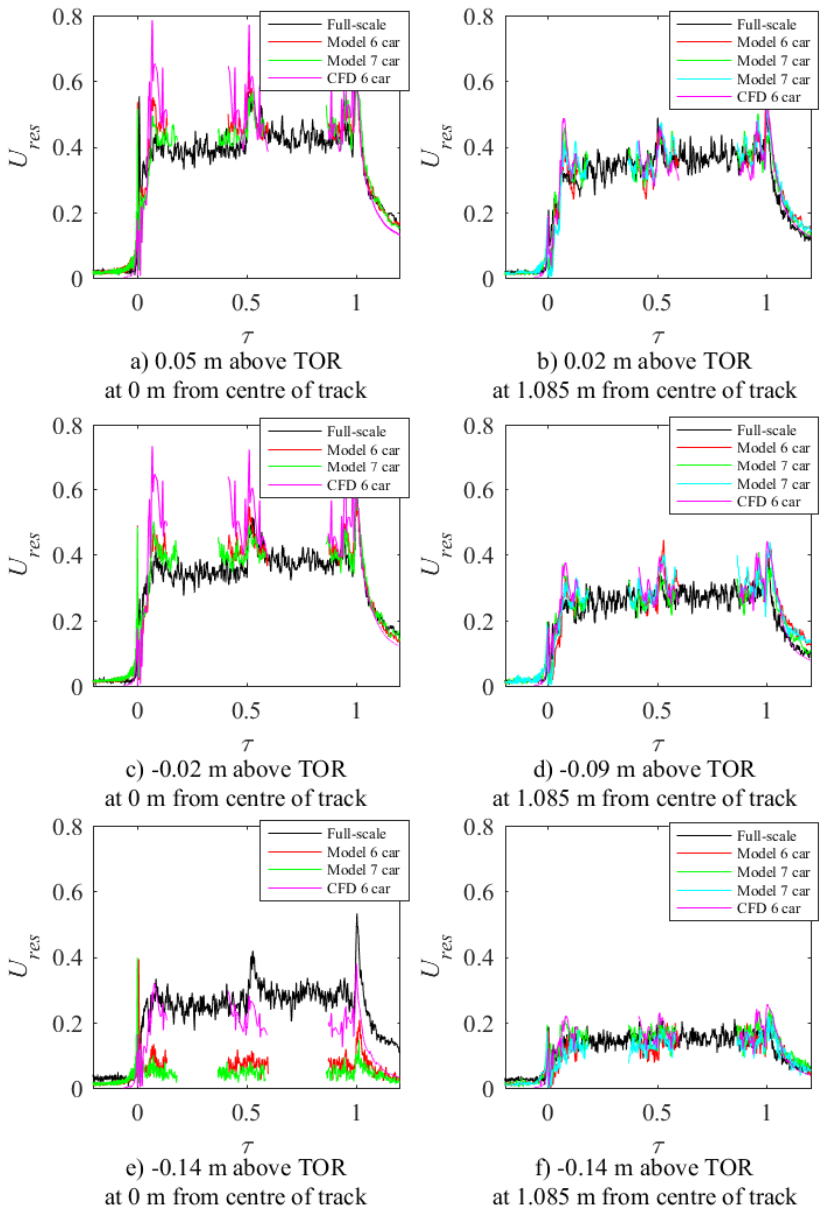

Figure 17: A comparison of ensemble averaged horizontal velocities, U_{res}, for CFD, full-scale and model-scale data for the rake of measuring positions at 0 m and 1.085 m from centre of track.

COT are shown for full-scale, model-scale and CFD data in figure 17. As noted previously there are small differences in measuring position between experimental studies. All model-scale positions are within 10% of the equivalent full-scale position. Again, as the train length in the scaled simulations is much shorter than at full-scale (7 versus 20 cars), data has been split in various locations and aligned with corresponding full-scale bogie and inter-carriage placements. The results in general exhibit very good agreement between all types of experiments and simulations. All results measured 1.085 m from COT lie within the bounds of experimental uncertainly ($\sim$2%). Model-scale results suggest that the flow is symmetrical for this particular train type.

Results measured at the COT show good agreement between model-scale and full-scale data for all positions measured, except at the lowest height (-0.14 m at full-scale). This discrepancy is due to the influence of the ground plane on the multi-hole probe. This effect is described in more detail in Lee et al. [26]. The multi-hole probe may also be affected by the large velocity gradients close to the wall. The probe operates on the assumption that the flow is uniform across the probe face (3.6 mm diameter). The full-scale data (figure 17) shows that the air speed is approximately 25% of the train speed just 60 mm above the ballast (which equates to 2.4 mm at model scale) and thus the assumption that the flow does not vary significantly across the probe head is clearly not valid in this region.

Conversely, CFD results exhibit agreement for the lowest measuring height but overshoot peak magnitudes at higher positions. The LES computational simulations are able to resolve turbulent scales within the flow to much greater detail than the measuring instrumentation can. One possible explanation was that the highly turbulent flow may result in large flow

angles which would cause the multi-hole and pitot-static probes to under-measure the flow velocity. However, the flow angles calculated from the CFD revealed that downstream of the train nose all of the flow remained within a $\pm 45^{\circ}$ window. The multi-hole probes additionally output a summary file containing mean flow yaw and pitch angles. The multi-hole probe data showed that flow was within $\pm 20^{\circ}$, agreeing with the average flow angle calculated in the CFD simulation, and therefore this is unlikely to be the cause. An alternative hypothesis is that the semi-porous ballast bed in experimental studies increases the friction coefficient at the flow boundary relative to that in the flat non-porous bed modelled in the CFD simulation. Dissipation of the energy of the flow within the ballast bed in the experimental studies may provide a mechanism to reduce velocity magnitudes which was not reproduced in the CFD simulations.

To gain a clearer understanding of the variation in turbulent slipstream velocities beneath the train, the standard deviation for different simulation techniques were compared with full-scale data. Figure 18 shows the ensemble mean velocity for the highest probe position above TOR at the COT, as well as the standard deviation above and below the ensemble, shown as a shaded band. It should be noted that simulation results are presented for longitudinal velocity U whereas the full-scale data is for U_{res}. Unfortunately, the instrumentation used at full-scale was unable to separate U and V components and as such a proper analysis of standard deviations was not possible. Additional analysis of simulation results for U and U_{res} found the magnitude of V was much lower than U and that standard deviations were similar for both major velocity components. Bounds for standard deviation about the ensemble mean are similar for all results and those are representative of all measuring positions. The average range of variation about

the mean is 15% for experiment measurements, increasing to 43%. Larger standard deviations occur in the CFD simulation due to ability of the CFD to resolve the flow to smaller scales than can be measured experimentally, thus increasing the uncertainty of measurements in relation to the ensemble mean. The results in figures 17 and 18 indicate that relatively good agreement is observed for ensemble means and standard deviations for all data sets; thus validating, by approved validation methodologies, the techniques used to model the flow underneath a high speed train.

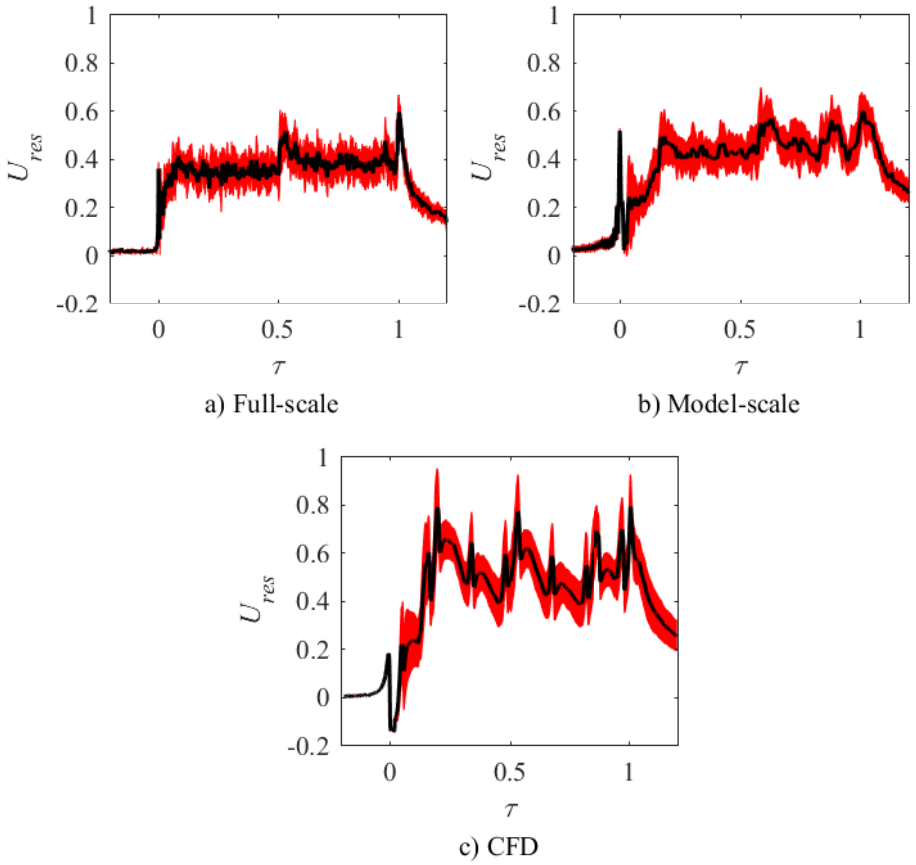

Figure 18: Ensemble longitudinal velocities U with bounds of plus/minus one standard deviation. The results are presented for all measurement techniques for the position 0.05 m above TOR at the COT.

	Height above top of rail (m)			
	-0.14	-0.09	-0.02	0.05
Full-scale	0.35	0.29	0.24	0.19
Modell-scale	1.27	0.40	0.25	0.21
CFD	0.27	0.32	0.28	0.42

Table 2: Average turbulence intensities calculated for the entire train length. Results are presented for increasing heights above TOR at the COT.

The ratio of standard deviation with the ensemble mean provides an approximation to the level of turbulence intensity at each measuring position. Mean turbulence intensities are compared in table 2. The level of turbulence intensity beneath the high speed train is high in comparison to results presented previously for measurements taken at the train side [12], but consistent in indicating a highly turbulent flow. Increased turbulence levels are due to exposed bogies and exposed intercarriage regions which effectively act as turbulence generators beneath the train. Turbulence intensities at model-scale and full-scale are similar, except for the lowest height (-0.14 m at full-scale). This discrepancy is due to the influence of the ground plane on the multi-hole probe. CFD values are slightly larger for higher measuring positions, due to the larger standard deviation values as discussed earlier, but lower for the lowest measuring position due to the smooth ground plane.

Flow development in figures 15-17 exhibit a clear influence from the underbody geometry of the train, with individual bogie types creating a clear effect on the aerodynamic flow. As with the pressure results, the standard and central type bogie configurations create a peak in slipstream velocities within the general boundary layer development. A smaller peak is observed for the articulated bogie between two carriages. Iso-surface plots from the CFD simulation, shown in figure 19, give a clearer indication of flow separation observed for the different bogie types. The double bogie configurations have a greater influence on the flow creating a larger number

of turbulent structures relative to the articulated bogie.

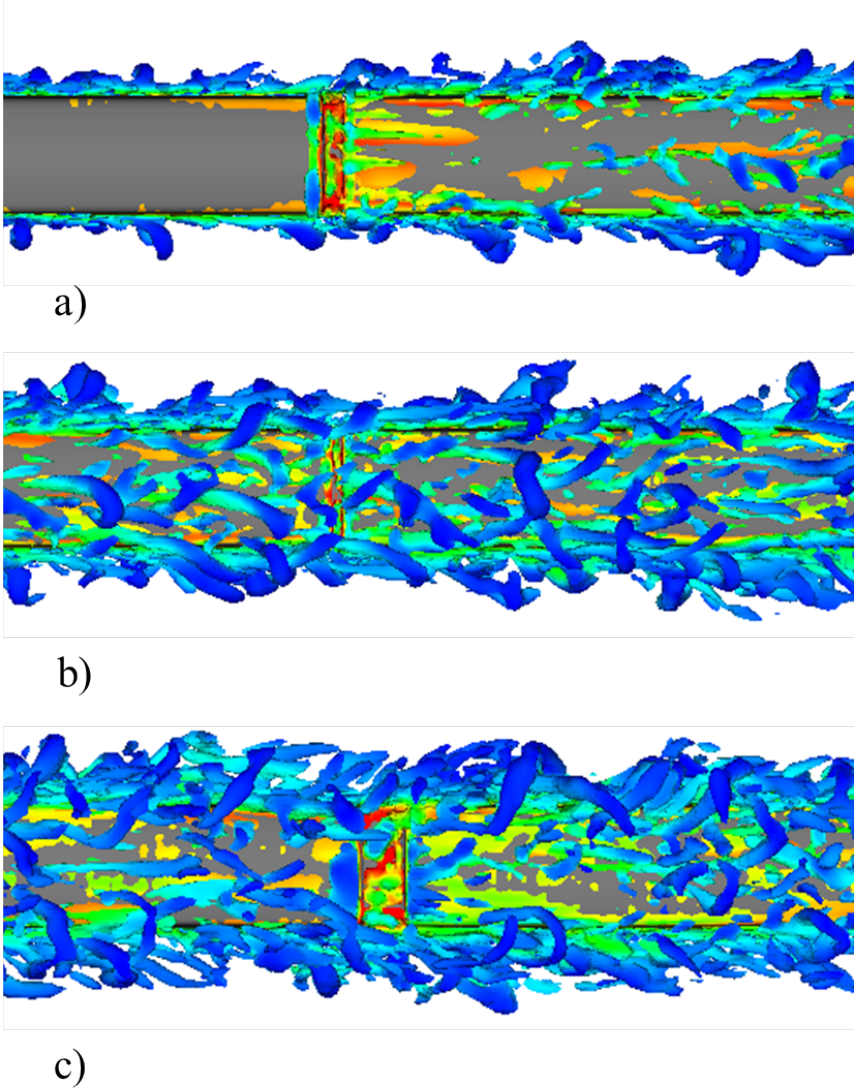

Figure 19: Iso-surfaces of Q-Criterion, Q=50,000, at a) standard, b) articulated and c) central intercarriage gaps.

The difference between aerodynamic flow development for the 6 and 7 car models is minimal, figure 20. Compared to full-scale data (figure 17) the results suggest that boundary layer stability, in terms of ensemble velocity magnitudes, is attained for the 6 car train and that the additional carriage

in the 7 car train has little influence on the aerodynamic flow development. Also shown in figure 20 is the effect of lateral position. As with pressure results, values measured outside the four foot have lower magnitude than values inside. Results from within the envelope of the train sides (Class 373 width is 2.81 m) all have a similar flow development with clear peaks relating to the intercarriage gaps and bogie placements. Measurements outside the train envelope have a much lower magnitude and the effect of key vehicle features is no longer clear. Once beyond the envelope of the train side the aerodynamic flow moves away from the COT in the general direction of lateral velocities, developing into the boundary layer flow measured at train side.

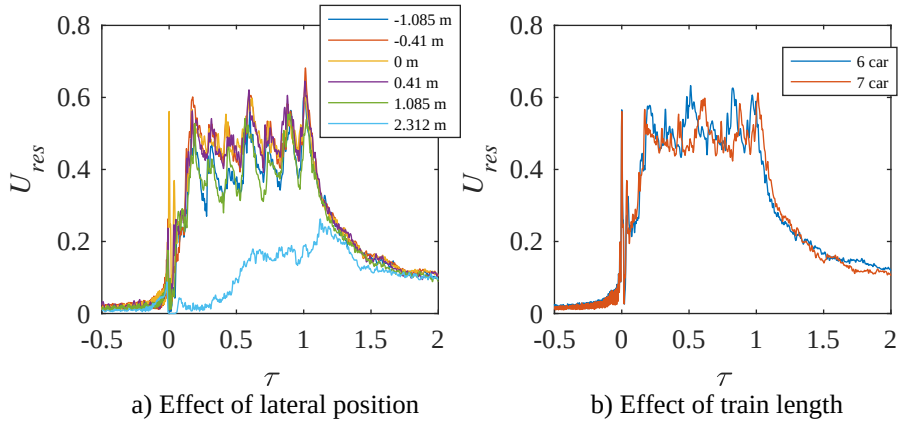

Figure 20: Comparison of model-scale 7 car total horizontal velocities U_{res} measured 0.1 m above top of rail for all lateral positions (a) and for the 6 and 7 car trains measured at the centre of track (b).

To fully validate the upside-down model-scale simulation it is important to analyse the aerodynamic flow further up the train side as well as underneath the train. Ensemble averaged total horizontal velocities 3 m from COT at a range of heights are shown in figure 21. Velocity magnitudes are higher at the lower measuring positions. This is likely due to the unshielded bogies creating a highly turbulent flow in contrast to the streamlined car-

riage walls sides at larger heights. The general flow development at the train side is comparable to results from other studies analysing high speed passenger trains [27, 25]. Results are further validated by comparison with full-scale data measured 0.2 m above TOR and 3.6 m from COT. The general flow development is similar as are the standard deviations; however, the full-scale ensemble average magnitudes are higher than the corresponding model-scale results. The magnitudes at this distance from COT are relatively low and issues may occur due to the multi-hole probe minimum flow cut-off condition and ambient atmospheric winds recorded at full-scale. A comparison with CFD data was not made because the absence of a ballast shoulder in the CFD simulation would have invalidated such a comparison [15].

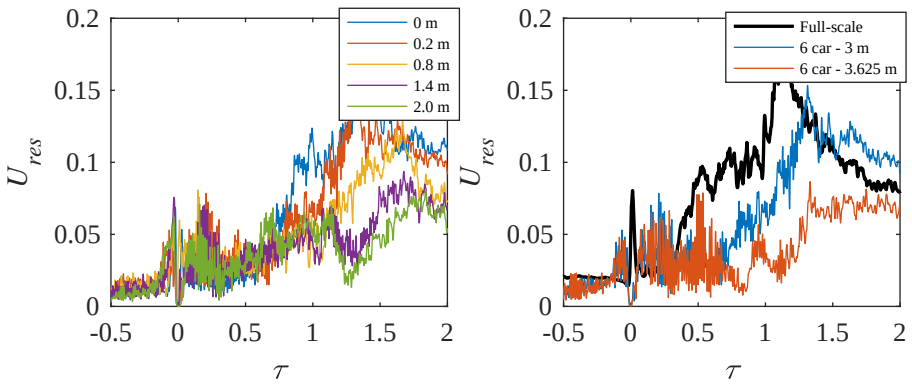

a) 3 m from COT b) 3.6 m from COT

Figure 21: Comparison of total horizontal velocities U_{res} measured 0.2 m above TOR at 3 m and 3.625 m from centre of track.

Analysis has so far focused on total horizontal velocities to gain an understanding of the shear effects on the ballasted trackbed. Vertical velocities may also be considered important to understand whether ballast particles are drawn upwards by slipstream velocities during the process of ballast projection. Data from both scaled simulations suggest velocities in the vertical direction typically have magnitudes less than 10% of the horizontal veloc-

ity. Generally vertical velocities were negative and thus act in the direction towards the trackbed, with only small positive velocity regions shown in the CFD simulations immediately after the train nose. It is concluded that vertical velocities have minimal effect on the ballasted trackbed and that any effects on ballast projection are likely to occur from a shear type flow.

6 Discussion

Ballast projection within the European Technical Specifications for Interoperability (TSI) is currently an open point. Limits on train aerodynamics are defined for pressure loading amplitudes on trackside structures, however this has not been extend to a standardised methodology and prescribed limit values for measured loads on the track bed [3]. The current need for train interoperability across national borders within a connected European rail network has led to the need for a set of practices for train homologation. In general train homologation is undertaken by conducting a series of experiments or simulations and comparing results to prescribed limits or previous results that were deemed satisfactory.

Full-scale experiments are generally expensive and difficult to conduct, and results are susceptible to changes in ambient conditions. Gauge limitations around the train prevent measurements from being made close to the train surface. Scaled simulations offer a cheaper and easier alternative method for understanding slipstream development in greater detail. The increased number of data points at model-scale can be supported by simulation of the entire flow field in CFD. However, due to issues such as scaling effects and differing methodologies, results need validation.

Ensemble averaged results from underneath the train presented in this paper show a good level of agreement between the simulation techniques and

full-scale data. Analysis of standard deviations, turbulence intensities and results further up the train side gave additional confidence in the validity of the model-scale and CFD simulations. The simulation techniques have therefore been proven to be as viable techniques for analysing the aerodynamic flow development beneath a high speed train and thus allowing for a greater understanding of the flow created and possible effects on the trackbed. It is conceivable that scaled simulations could provide a suitable means to assess limits on underbody flow for train homologation.

There were however a number of limitations highlighted in the analysis. Multi-hole probes were found to be unsuitable very close to the ballast layer. Other instruments such as hot-wires or laser anemometers may alleviate some of these issues and provide greater detail close to the trackbed. CFD was shown to offer the ability to examine in detail flow features that were identified in the experimental studies; however, greater detail would be needed in the simulation to fully resolve all of the effects identified in the experiments. Results suggested that a level of porosity and increased surface roughness were required to model the dispersion of energy from the flow at the trackbed boundary. The addition of such complexities would dramatically increase the computational power and time costs when running LES simulations.

7 Conclusions

An in-depth study to analyse the performance of different methods for simulating the aerodynamic flow development beneath a high speed train has been undertaken. Both physical and numerical simulation techniques were validated against data from a series of full-scale experiments. A thorough discussion of different simulation techniques highlighted the pros and cons

of each technique and where possible suggestions were made about how to improve the modelling in future. It was shown that both simulation techniques could be used to further the understanding of the aerodynamic flow development beneath a high speed train with a view to providing detailed results to aid the understanding of the processes which induce ballast projection. It is clear that a number of important conclusions can be drawn from this study.

- It is possible to measure the aerodynamic flow development beneath an upside-down moving model train passing beneath a suspended simulated ground plane. The technique provided repeatable and accurate values of flow velocities and static pressures in the vicinity of the trackbed.

- It was shown that CFD simulations could be used as a method to model the flow beneath a high speed train. Although the LES simulation gave highly converged solutions with over 90% of the TKE being resolved, it was shown that further work is needed to ensure the solutions agree well with experimental data.

- The aerodynamic flow development was shown to be similar to results measured previously at train side, as well as previous measurements made underneath a high speed train. The characteristic flow could be divided into a number of key flow regions relating to the train nose, intercarriage/bogie regions and train tail.

- Comparison of all results with a series of full-scale measurements demonstrated good agreement for all measurement positions for both pressure and velocity data. The majority of data were found to lie within experimental uncertainty bounds and within two standard de-

viations of the ensemble mean time history. This comparison can be considered to validate the different simulation techniques.

- Pressure coefficients were greater in the CFD simulation than in the experimental studies. This was suggested to be because the experimental results contained ballast stones creating a diffusive effect whereas the flow in the CFD simulations stagnated on a smooth non-porous surface.

- Horizontal velocities measured close to the trackbed at model-scale were found to be much lower than results recorded at a similar position in the full-scale tests. A thorough discussion of the experimental technique suggested that the multi-hole probe gave unreliable results when in close proximity to the ballasted surface. CFD results for horizontal velocities within the four foot were found to overshoot full-scale results. This was again thought to be related to the influence of ballast stones in the experimental studies.

- Different bogie types clearly influence the aerodynamic flow beneath the train, with smaller pressure and velocity magnitudes recorded for the articulated bogie relative to standard and central bogies.

- The effect of train length (over the ranges tested in this study) was found to be negligible.

- Model-scale measurements made outside the four foot further up the train side were shown to agree with full-scale data.

- 1/25th scale simulations were demonstrated to be an appropriate method to model underbody flow with a view to train homologation.

Acknowledgements

The work in this paper was funded by EPSRC project EP/K037676/1. The authors would like to thank NRHS for their assistance with the full-scale experiments and Eurostar International Ltd for their cooperation throughout the project.

References

[1] H. B. Kwon and C. S. Park. An experimental study on the relationship between ballast flying phenomenon and strong wind under high speed train. In *Proceedings of the World Congress on Rail Research, Montreal, Canada*, 2006.

[2] A. D. Quinn, M. Hayward, C. J. Baker, F. Schmid, J. A. Priest, and W. Powrie. A full-scale experimental and modelling study of ballast flight under high-speed trains. *Proceedings of the Institution of Mechanical Engineers, Part F: Journal of Rail and Rapid Transit*, 224(2):61–74, 2010.

[3] TSI. COMMISSION REGULATION (EU) No 1302/2014 concerning a technical specification for interoperability relating to the rolling stock - locomotives and passenger rolling stock subsystem of the rail system in the European Union. Technical report, Official Journal of the European Union, 2014.

[4] A Ido, S Saitou, K Nakade, and S Iikura. Study on under-floor flow to reduce ballast flying phenomena. In *World Congress on Rail Research, Seoul, Paper*, number S2, pages 3–4, 2008.

[5] P. Deeg, M. Jönsson, H.J. Kaltenbach, M. Schober, and M. Weise. Cross-comparison of measurement techniques for the determination of

train induced aerodynamic loads on the track bed. In *Proceedings of the BBAA VI, Milano, Italy*, 2008.

[6] H. J. Kaltenbach, P. E. Gautier, G. Agirre, A. Orellano, K. Schroeder-Bodenstein, M. Testa, and T. H. Tielkes. Assessment of the aerodynamic loads on the trackbed causing ballast projection: results from the DEUFRAKO project Aerodynamics in Open Air (AOA). In *Proceedings of the World Congress on Rail Research, Seoul, South Korea*, 2008.

[7] A. Ido and S. Yoshioka. Development of a model running facility for a study on under-floor flow. *Journal of Mechanical Systems for Transportation and Logistics*, 3:294–304, 2010.

[8] G. Diana, D. Rocchi, G. Tomasini, P. Schito, and A. Premoli. Full scale experimental analysis of train induced aerodynamic forces on the ballast of Italian high speed line. In *International Workshop on Railway Aerodynamics at the University of Birmingham*, 2013.

[9] B. J. Lazaro and E. Gonzalez. Characterization and modeling of flying ballast phenomena in high-speed train lines. In *The ninth world congress on railway research*, 2010.

[10] F. Navarro Medina, S. Andres, A. Pedro, M. I. Pérez Grande, A. Martínez Muelas, E. Vega Ramiro, M. Rodriguez Plaza, I. J. Iglesias Dia, A. Andres Alguacil, and D. Alonso Gimeno. The ballast pick-up problem. A theoretical approach and two experimental campaigns. 2011.

[11] F. Navarro-Medina and I. Perez-Grande. Comparative study of the effect of several trains on the rotation motion of ballast stones. *Pro-*

ceedings of the Institution of Mechanical Engineers, Part F: Journal of Rail and Rapid Transit, 229(1):71–88, 2015.

[12] C. J. Baker. The flow around high speed trains. *Journal of Wind Engineering and Industrial Aerodynamics*, 98(6-7):277 – 298, 2010. 6th International Colloquium on Bluff Body Aerodynamics and Applications.

[13] C. J. Baker, D. Soper, D. Flynn, A. Jackson, D. R. Milne, L. Le Pen, J. Zhu, Z. Hu, and W Powrie. Full scale measurements of train underbody flows and track forces. *Journal of Wind Engineering and Industrial Aerodynamics*, 2017.

[14] C. J. Baker, S. J. Dalley, T. Johnson, A. D. Quinn, and N. G. Wright. The slipstream and wake of a high-speed train. *Proceedings of the Institution of Mechanical Engineers, Part F: Journal of Rail and Rapid Transit*, 215(2):83–99, 2001.

[15] D. Soper, M. Gallagher, C. J. Baker, and A. D. Quinn. A model-scale study to assess the influence of ground geometries on aerodynamic flow development around a train. *Proceedings of the Institution of Mechanical Engineers, Part F: Journal of Rail and Rapid Transit*, 2016.

[16] C. J. Baker, D. Soper, D. Flynn, A. Jackson, D. R. Milne, L. Le Pen, J. Zhu, Z. Hu, and W Powrie. Ballast flight under high-speed trains - aerodynamic and geotechnical studies. In *Stephenson conference London 2017*, 2017.

[17] TFI. Turbulent Flow Instrumentation - Cobra Probe - Getting started guide. Technical report, Turbulent Flow Instrumentation, 2011.

[18] CEN. EN 14067-4 Railway applications - Aerodynamics Part 4: Requirements and test procedures for aerodynamics on open track. Technical report, CEN, 2009.

[19] S. Huang, H. Hemida, and M. Yang. Numerical calculation of the slipstream generated by a CRH2 high-speed train. *Proceedings of the Institution of Mechanical Engineers, Part F: Journal of Rail and Rapid Transit*, 230(1):103–116, 2016.

[20] D. Flynn, H. Hassan, D. Soper, and C. J. Baker. Detached-eddy simulation of the slipstream of an operational freight train. *Journal of Wind Engineering and Industrial Aerodynamics*, 132:1–12, 2014.

[21] H. Hemida, C. J. Baker, and G. Gao. The calculation of train slipstreams using large-eddy simulation. *Proceedings of the Institution of Mechanical Engineers, Part F: Journal of Rail and Rapid Transit*, page 0954409712460982, 2012.

[22] P. K. Sweby. High resolution schemes using flux limiters for hyperbolic conservation laws. *SIAM journal on numerical analysis*, 21(5):995–1011, 1984.

[23] C. Zhu, H. Hemida, D. Flynn, C. J. Baker, X. Liang, and D. Zhou. Numerical simulation of the slipstream and aeroacoustic field around a high-speed train. *Proceedings of the Institution of Mechanical Engineers, Part F: Journal of Rail and Rapid Transit*, page 0954409716641150, 2016.

[24] S. B. Pope. *Turbulent flows*. IOP Publishing, 2001.

[25] C. J. Baker, A. Quinn, M. Sima, L. Hoefener, and R. Licciardello. Full-scale measurement and analysis of train slipstreams and wakes. Part

1: Ensemble averages. *Proceedings of the Institution of Mechanical Engineers, Part F: Journal of Rail and Rapid Transit*, 228(5):451–467, 2014.

[26] S. W. Lee and T. J. Yoon. An investigation of wall-proximity effect using a typical large-scale five-hole probe. *KSME International Journal*, 13(3):273–285, 1999.

[27] G. Mancini and A. Malfatti. *Full scale measurements on high speed train ETR 500 passing in open air and in tunnels of Italian high speed line*, pages 101–122. Springer Berlin Heidelberg, Berlin, Heidelberg, 2002.